RSC Advances

PAPER

View Article Online
View Journal | View Issue

Cite this: *RSC Adv.*, 2014, **4**, 9401

A dual-functional additive improves the performance of molecular bulk heterojunction photovoltaic cells†

Mahmoud E. Farahat,[abc] Hung-Yu Wei,[d] Mohammed Aziz Ibrahem,[bce] Karunakara Moorthy Boopathi,[ac] Kung-Hwa Wei[f] and Chih-Wei Chu*[bg]

Received 20th November 2013
Accepted 6th December 2013

DOI: 10.1039/c3ra46884d

www.rsc.org/advances

In this paper we report a simple and effective approach towards improving the performance of molecular bulk heterojunction (BHJ) photovoltaics through incorporation of a new, nonvolatile processing additive; (3-chloropropyl)trimethoxysilane (CP3MS). A small amount of the additive CP3MS combined with post-annealing treatment significantly enhanced the power conversion efficiency (PCE) of dialkylated diketopyrrolopyrrole chromophore (SMDPPEH)-based molecular BHJ solar cells. The PCE increased from 2.75% for a device prepared without the additive or annealing to 4.55% for a device containing 0.1% CP3MS that had been subjected to post-annealing treatment at 100 °C for 10 min. CP3MS performed an interesting dual function when incorporated as an additive in molecular BHJ devices. The first was that it controlled the morphology: the addition of 0.1% CP3MS to the SMDPPEH:$PC_{61}BM$ blend was sufficient to improve the film's crystallinity and morphology. The second function was the spontaneous migration of the CP3MS molecules from the bulk to the interface between the active layer and the Al cathode, forming an ultrathin interlayer that acted as a buffer layer suppressing charge recombination and enhancing charge transport at the interface. Analyses using atomic force microscopy, X-ray diffraction, and X-ray photoelectron spectroscopy, together with examinations of device performance, confirmed the dual-functional nature of CP3MS as an additive. CP3MS also showed its promising ability to enhance the performance of different blend systems. The performance of benzodithiophene (BDT)-based molecular solar cells enhanced from 3.05% without additive to 3.8% with the incorporation of 0.1% CP3MS.

1. Introduction

The need for eco-friendly, cost-effective, and sustainable energy sources is boosting the development of solar energy. Bulk heterojunction (BHJ) organic photovoltaics are considered to be among the most promising low-cost solar energy technologies.[1–3] Solution-processable BHJ organic photovoltaics are required for the possibility of large-scale, inexpensive fabrication on flexible substrates.[3–5] In BHJ organic photovoltaics, both polymers[4] and small molecules[5–9] are commonly used as donor materials. Small molecules, however, have several advantages over polymeric counterparts: well-defined molecular structures and molecular weights; ready modification and functionalization; lack of end group contaminants; simple mass-scale production and purification; high charge carrier mobilities, due to their greater tendency to self-assemble into ordered domains; and good batch-to-batch reproducibility.[6] The power conversion efficiencies (PCEs) of polymer-based BHJ solar cells have improved significantly over the last decade, reaching values exceeding 10.6% for tandem cells[10] and near 9.2% for single cells.[11] Among molecular BHJ solar cells, Heeger's group recently achieved a record high PCE of 8.9%.[12]

In BHJ organic solar cells, morphology is an issue of great interest because it significantly impacts device performance. The formation of interpenetrating networks of donors and acceptors having feature dimensions on the order of 10 to 20 nm is attractive for improved charge separation.[13–15] Several techniques have been applied to achieve such well-defined morphologies for charge diffusion, separation, and transfer: thermal annealing (both pre-[16,17] and post-[18–21] annealing),

[a]*Department of Engineering and System Science, National Tsing-Hua University, Hsinchu 30013, Taiwan (Republic of China)*

[b]*Research Center for Applied Sciences, Academia Sinica, Taipei 115, Taiwan (Republic of China). E-mail: gchu@gate.sinica.edu.tw*

[c]*Nanoscience and Technology Program, Taiwan International Graduate Program, Academia Sinica, Taipei 115, Taiwan (Republic of China)*

[d]*Institute of Polymer Science and Engineering, National Taiwan University, Taipei, 10617, Taiwan (Republic of China)*

[e]*Department of Physics, National Taiwan University, Taipei 106, Taiwan (Republic of China)*

[f]*Department of Materials Science and Engineering, National Chiao Tung University, 1001 Ta Hsueh Road, Hsinchu, 30050, Taiwan (Republic of China)*

[g]*Department of Photonics, National Chiao Tung University, Hsinchu 300, Taiwan (Republic of China)*

† Electronic supplementary information (ESI) available. See DOI: 10.1039/c3ra46884d

solvent vapor annealing,[22] facile aqueous solution treatment,[23] selection of appropriate casting solvents,[24,25] controlling surface energy,[26,27] and the use of additives[28–36] are commonly employed to control the morphologies of photoactive layers in organic solar cells. Combining the effects of thermal annealing and additives is also a useful approach.[37,38] Although the use of additives can be an effective means of controlling morphologies, the same additive can have different effects in different blending systems. For example, DIO has a positive effect when added to the PCPDTBT/$PC_{71}BM$ blend system,[28] but a negative effect when added to the TQ1:$PC_{71}BM$ blend system.[35] These different effects result from the different interactions of the additive units with the components of the different blends.

For processing additives to be used effectively in BHJ organic solar cells, two criteria must be fulfilled: (i) the additive should have a boiling point higher than that of the host solvent; (ii) the additive should have different solubility tendencies toward the donor (polymer or small molecule) and acceptor (usually a fullerene), resulting in the desired phase separation occurring while the film is drying.[24,28,33] Processing additives might be classified as volatile and nonvolatile. Bazan and coworkers reported that there was no significant content of the additive (dithiol) in the film after drying under vacuum (*ca.* 10^{-3} torr) for 10 min at room temperature, suggesting that the additive was volatile.[36,37] Nonvolatile additives that control the morphology have also been reported. Loo and coworkers reported that the degree of phase separation was related to the hydrophobicity of the nonvolatile additive.[39] Kim and coworkers studied the effect of adding 2% of a hydrophobic end-functionalized P3HT (F-P3HT) as a nonvolatile additive to control the morphology of a P3HT:PCBM blend.[40] Nonvolatile additives can also act as a buffer layer, formed through spontaneous migration to the interface between the active layer and the metal cathode. Hashimoto and coworkers synthesized a fullerene derivative presenting a fluorocarbon chain (F-PCBM) and used it as an additive in a BHJ of P3HT:$PC_{60}BM$; they attributed the improvement in cell performance, particularly in terms of the fill factor (FF), to the formation of a thin buffer layer through spontaneous migration of F-PCBM at the interface between the Al cathode and the active layer.[41] Similar phenomena have been observed when using poly(ethylene glycol)[42,43] and fullerene-end-capped poly(ethylene glycol)[44] as additives. When using poly(ethylene glycol) as the additive in a BHJ organic solar cell, drying of the polymer blend led to the additive PEG polymers in the active layer spontaneously migrating to the interface between the Al cathode and the active layer, achieving a thermodynamic equilibrium and serving as a natural buffer layer. The PEG nano-interlayer effectively modifies the work function of the Al electrode and decreases the contact resistance between the active layer and the metal cathode.[42,43] When polydimethylsiloxane-*block*-poly(methyl methacrylate) (PDMS-*b*-PMMA) was used as an additive in a P3HT:PCBM blend system, an ultrathin buffer layer of PDMS-*b*-PMMA spontaneously formed at the interface between the active layer and the metal cathode, as confirmed using X-ray photoelectron spectroscopy (XPS).[45] This self-organized interfacial layer improved the PCE of the devices and confirmed the possibility of spontaneous migration of silane-based additives.[33]

To the best of our knowledge, processing additives that have been used in organic photovoltaics showed only one function; either controlling the morphology or spontaneously migrating to the surface to form a buffer layer at the interface. However in our work here, we report for the first time a new additive with a dual-function nature. We report an effective approach toward improving BHJ cell performance through the incorporation of a new nonvolatile additive, CP3MS. A small amount of CP3MS combined with post-annealing treatment significantly enhanced the PCE in diketopyrrolopyrrole (DPP)-based molecular BHJ solar cells. The PCE increased from 2.75% for a device prepared without the additive or annealing to 4.55% for a device containing 0.1% of the CP3MS additive followed by post-annealing treatment at 100 °C for 10 min. CP3MS incorporated as an additive in SMDPPEH:$PC_{61}BM$ BHJ molecular solar cells revealed an interesting dual-functional behavior. The first function is its ability to control the morphology. The incorporation of 0.1% CP3MS as an additive inside the blend was sufficient to enhance the film morphology and crystallinity, as revealed using atomic force microscopy (AFM) and X-ray diffraction (XRD). The second function is the spontaneous migration of CP3MS to the interface between the active layer and the Al metal cathode, forming an ultrathin interlayer that acted as a buffer layer suppressing charge recombination and enhancing charge transport at the interface. We confirmed the presence of this ultrathin interlayer of CP3MS at the interface through XPS and AFM measurements. AFM, XRD, and XPS, together with measurements of device performance, confirmed the novel concept of the dual-functional nature of CP3MS incorporated in BHJ SMDPPEH:$PC_{61}BM$ blend systems. CP3MS also showed a promising ability to enhance the performance of different blend systems. The performance of benzodithiophene (BDT)-based molecular solar cells enhanced from 3.05% without additive to 3.8% with the incorporation of 0.1% CP3MS.

2. Results and discussion

2.1. Device performance

DPP-based semiconductors are a class of promising candidates in optoelectronics.[48,49] For solution-processed BHJ organic solar cells, Nguyen's group performed an intensive and detailed study of the development of DPP-based small molecules.[5,31,50–54] They achieved an efficiency of 4.8% when using a DPP$(TBFu)_2$:$PC_{71}BM$ blend system[52] and 5.2% with a DPP$(TBFu)_2$:$PC_{61}BM$ blend system.[55] Recently they also reported a PCE of 5.5% with a tri-diketopyrrolopyrrole after processing with chloronaphthalene (CN) as an additive.[56] These efficiencies are the highest ever reported when using DPP-based, solution-processed small molecules. A few other studies have also revealed PCEs near 4% for DPP-based molecular solar cells.[57,58] Using a dialkylated diketopyrrolopyrrole chromophore (SMDPPEH) as a donor material, the Nguyen group achieved PCEs of 3% and 2.93% after blending with $PC_{71}BM$[59] and $PC_{61}BM$,[60] respectively.

Scheme 1 displays the chemical structures of the materials tested in this study: SMDPPEH as the donor, $PC_{61}BM$ as the

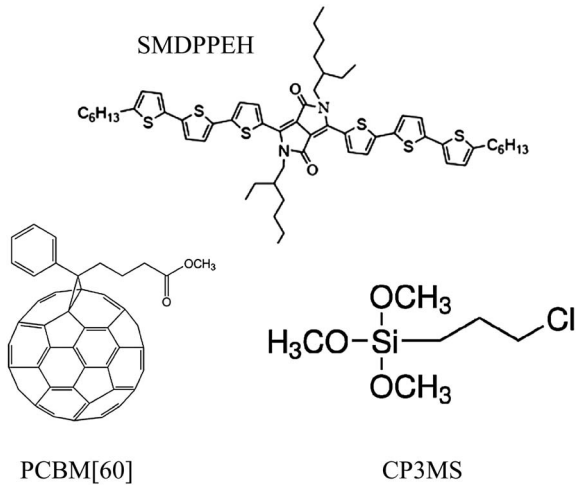

Scheme 1 Molecular structures of chemicals used in the study: SMDPPEH (donor), PCBM[60] (acceptor) and the CP3MS (additive).

acceptor, and CP3MS as the processing additive. For comparison, we prepared devices under four different conditions: (i) without any additive or any thermal annealing ("as-cast"); (ii) without any additive, but post-annealed at 100 °C for 10 min ("post-annealing-only"); (iii) with 0.1% CP3MS as an additive, but without any thermal annealing ("additive-only"); and (iv) with 0.1% CP3MS, followed by post-annealing at 100 °C for 10 min ("combined effect"). We chose these conditions after detailed optimization, as discussed later in this section. The photovoltaic characteristics of these devices (Fig. 1a, Table 1) revealed that the short-circuit current (J_{sc}) was significantly enhanced under all conditions (highest value: 12.36 mA cm^{-2}) relative to those previously reported for devices incorporating SMDPPEH as the donor material (highest value: 8.06 mA cm^{-2}).[60] The increase in the value of J_{sc} might have arisen mainly from the use of chlorobenzene (CB) as a solvent, instead of chloroform as in the previous studies. The effect of the selected solvent on the PCE, in general, and the value of J_{sc}, in particular, has been described in many previous reports.[24,25] The enhanced value of J_{sc} together with the significant increase in the FF led to the significant gain in PCE. The FF of the device prepared under the "as-cast" conditions was 38.66%, providing a PCE of 2.75%; the device prepared under the "combined effect" conditions increased the FF to 51.14%, leading to a PCE of 4.55%. This latter PCE is the highest reported for a device incorporating SMDPPEH; it was achieved by combining effects of the additive CP3MS and post-annealing treatment. Notably, however, each of these effects had its own significant role in enhancing the overall PCE of the devices based on SMDPPEH:$PC_{61}BM$. The devices prepared under the "post-annealing-only" and "additive-only" conditions clearly revealed the independent influences of post-annealing and the additive on the overall performance.

Annealing the full device after deposition of the Al cathode (post-annealing) led to a significant enhancement in PCE, mainly due to a significant increase in the FF. We tested the performance of devices that we had annealed at different

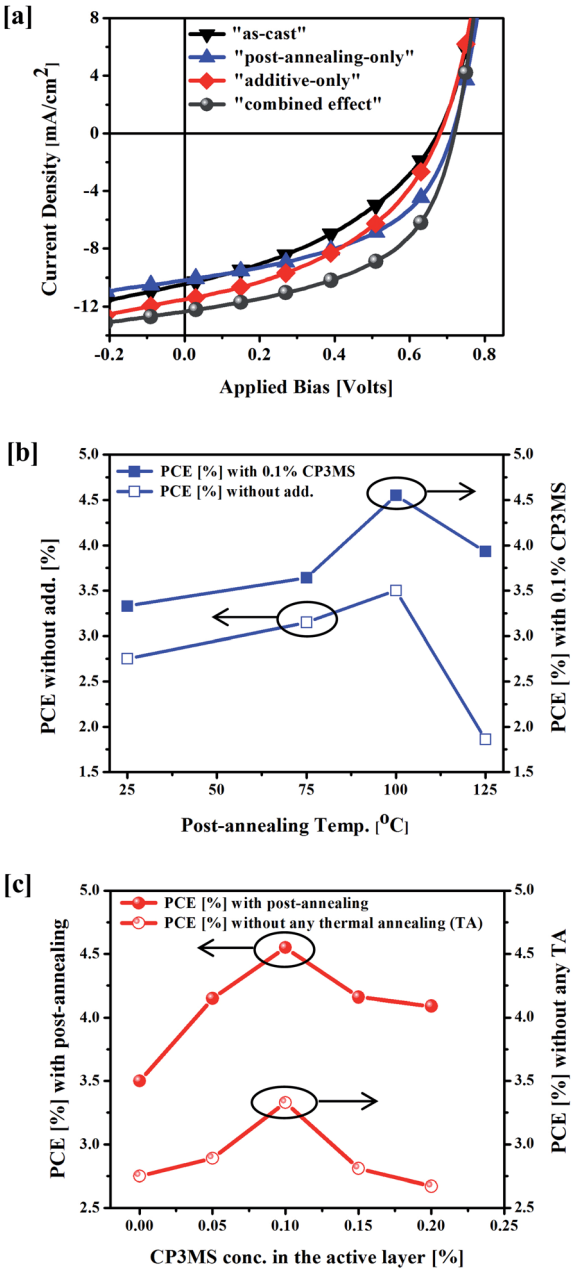

Fig. 1 (a) J–V characteristics of the devices, revealing their best performances under different conditions. (b) PCEs of devices, prepared with and without the additive, that had been subjected to various post-annealing temperatures. (c) PCEs of devices, prepared with and without post-annealing, incorporating different concentrations of CP3MS.

Table 1 Photovoltaic characteristics of devices exhibiting the best PCEs under different treatment conditions

Treatment conditions	J_{sc} [mA cm^{-2}]	V_{oc} [V]	FF [%]	PCE [%]	R_s [Ω cm^2]
"as-cast"	10.46	0.68	38.66	2.75	2.15
"additive-only"	11.52	0.68	42.51	3.33	1.77
"post-annealing-only"	10.20	0.71	48.33	3.50	1.85
"combined effect"	12.36	0.72	51.14	4.55	1.68

post-annealing temperatures (75, 100, or 125 °C; Fig. S1 and Table S1, ESI†) and for different post-annealing periods (10, 20, 30, or 40 min; Fig. S2 and Table S2, ESI†). The highest PCE under the conditions of "post-annealing-only" was that obtained for the device annealed at 100 °C for 10 min; we used these optimized conditions for our subsequent investigations. The device prepared under these conditions exhibited a PCE of 3.5% with a significant enhancement in the FF of 48.33% and an enhanced value of V_{oc} of 0.71 V relative to those values (PCE = 2.75%; FF = 38.66%; V_{oc} = 0.68 V) for the device formed under the "as-cast" conditions. The improvements in FF and the value of V_{oc} after post-annealing treatment suggests the formation of a pinhole-free interface between the Al metal cathode and the active layer (active layer–Al interface). Table 2 and Fig. S3 (ESI†) reveal the influence of CP3MS as an additive in the SMDPPEH:$PC_{61}BM$ blend system. We investigated the effect of different CP3MS concentrations (0.05–0.2%) on the performance of devices prepared under the optimized post-annealing conditions (100 °C, 10 min). Although all of the tested concentrations of CP3MS, followed by post-annealing, led to significant enhancements in the overall performance, the highest PCE (4.55%) was achieved after incorporating 0.1% CP3MS, with simultaneously enhanced values of J_{sc} (12.36 mA cm^{-2}) and of the FF (51.14%). Fig. 1b and c summarize the effects of both post-annealing and the additive concentration on the device performance respectively. Combining the effects of post-annealing treatment with a small amount (0.1%) of the additive CP3MS enhanced the PCE of the SMDPPEH:$PC_{61}BM$ system by 55.3% relative to the value reported previously for a device featuring the same system.[60] In the Morphology section below, we describe in more detail the effect of post-annealing and/or the additive CP3MS on the morphology of the active layer and on the interface between the active layer and Al metal cathode.

Absorbance measurements of films of pure SMDPPEH and SMDPPEH:$PC_{61}BM$, prepared with and without the additive, revealed broad absorbance over the entire visible region up to approximately 800 nm (Fig. 2a). The spectrum of pure SMDPPEH features three absorption peaks at 416, 648, and 720 nm; we attribute the first to π–π* transitions in both the DPP and thiophene units, the second to intramolecular charge transfer transitions between the DPP and oligothiophene units, and the third to transitions involving an aggregate species brought about by the strong intermolecular interactions similar to those observed for highly ordered oligothiophene–DPP systems. Blending SMDPPEH with fullerene led to this aggregate absorption band being slightly blue-shifted relative to that of the film of pure SMDPPEH, indicating a disruption of the donor packing upon the addition of the fullerene molecules, which is consistent with previous reports.[17,60] A fourth peak, at 337 nm, attributable to fullerene absorption, appeared for the films cast from the blend in the presence or absence of CP3MS. The incorporation of the additive slightly affected the absorption of the films cast from the blend, but there were no significant differences in these spectra. Correlating the values of J_{sc} and the absorption spectra, the external quantum efficiencies (EQEs) increased significantly over the entire wavelength range from 300 to 800 nm for the devices prepared under the conditions of "post-annealing-only" and "combined effect" relative to that of the "as-cast" device. In Fig. 2b, the EQE spectrum for the "post-annealing-only" device features a peak of 50% at 645 nm, compared with a value of 43% at 650 nm for the "as-cast" device, whereas the device prepared under the "combined effect" conditions gave an EQE of 55% at 640 nm. These EQEs are consistent with the absorption spectra and the values of J_{sc}

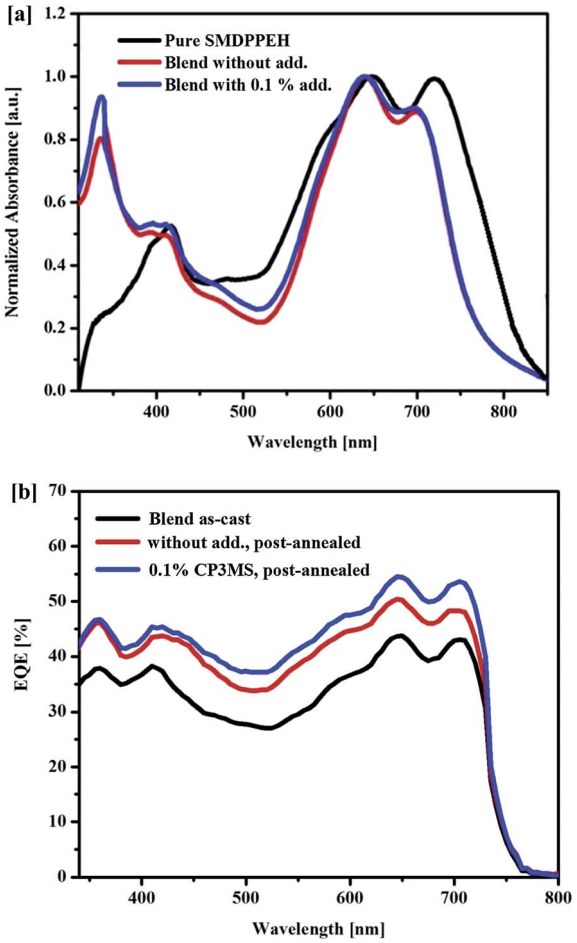

Fig. 2 (a) Normalized UV-vis absorption spectra of pure SMDPPEH and SMDPPEH:$PC_{61}BM$ blends with and without incorporation of CP3MS and (b) EQE spectra of SMDPPEH:$PC_{61}BM$ blends that had been subjected to various treatment conditions.

Table 2 Effect of different concentrations of CP3MS on device performance under the conditions of post-annealing treatment at 100 °C for 10 min

Treatment conditions	J_{sc} [mA cm^{-2}]	V_{oc} [V]	FF [%]	PCE [%]
"post-annealing-only"	10.20	0.71	48.33	3.50
0.05% CP3MS	12.13	0.71	48.19	4.15
0.10% CP3MS	12.36	0.72	51.14	4.55
0.15% CP3MS	11.76	0.73	48.46	4.16
0.20% CP3MS	11.55	0.72	49.18	4.09

obtained from the *J–V* curves, suggesting that both post-annealing and application of the additive improved the nano-scale phase separation between the SMDPPEH and $PC_{61}BM$ components, leading to well-connected, percolated pathways of each phase-separated component.

2.2. Crystallinity, morphology, and interface

We used conventional XRD to study the influences of the additive and thermal annealing on the molecular packing and degrees of crystallinity of the active layers (Fig. 3). The XRD pattern of the "additive-only" active layer indicated that the incorporation of a small amount (0.1%) of CP3MS resulted in higher crystallinity compared to that in the "as-cast" samples. Active layers containing 0.1% CP3MS provided a better-defined diffraction signal at a value of 2θ of 21.46°, which corresponds to a π–π stacking distance of 0.41 nm. We also detected a signal at a value of 2θ of 5.84°, giving a *d*-spacing between the alkyl chains of 1.5 nm. These results are consistent with the increase in the value of J_{sc} and FF after the addition of a small amount of CP3MS, confirming its role as an additive that enhances the crystallinity of the active layers, even in the absence of any thermal annealing. For samples prepared under "post-annealing-only" conditions, the crystallinity of the films of the active layers exhibited improved crystallinity, with slightly tighter packing giving a shorter *d*-spacing between the alkyl chains of 1.38 nm, corresponding to a value of 2θ of 6.36°, while the π–π stacking distance remained the same (2θ = 21.46°). Devices prepared under "combined effect" conditions also improved the crystallinity with a slight shift in the value of 2θ to 6.24°, giving a *d*-spacing between the alkyl chains of 1.41 nm, while the π–π stacking distance remained the same (2θ = 21.46°). The XRD results are consistent with the device performance data, where the increases in the FF and the values of J_{sc} can be explained in terms of the enhanced crystallinity of the devices, due to the effects of the incorporated additive and/or thermal annealing.[17]

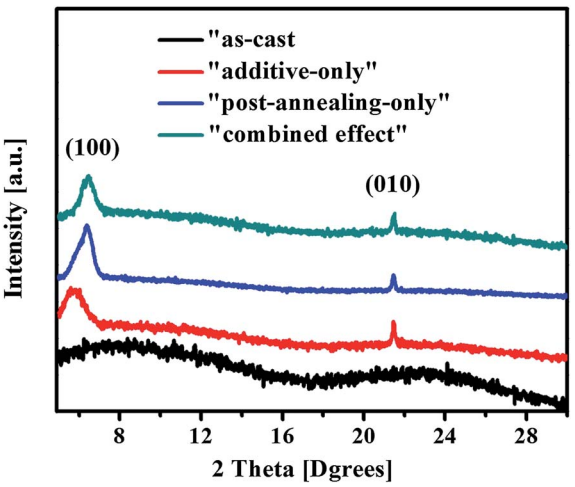

Fig. 3 XRD patterns of SMDPPEH:$PC_{60}BM$ active layers prepared using different treatment conditions.

Furthermore, we used AFM (tapping mode) to examine the effects of post-annealing and the additive on the morphologies of the active layers. Fig. 4 displays height and corresponding phase images of the films prepared under the four conditions: "as-cast," "additive-only," "post-annealing-only," and "combined effect." To investigate the morphologies of the active layers after post-annealing, we removed the Al cathodes using sticky-tape.[18,19] Interestingly, the devices prepared without post-annealing with or without the additive ("as-cast" and "additive-only") resulted in complete removal of the active layer during the peeling-off of the Al cathode. In contrast, the Al cathodes on top of the post-annealed devices with or without the additive ("post-annealing-only" and "combined effect") were readily taken off without removing the active layer (see Fig. S4, ESI†). This behavior might be attributable primarily to the positive effect of post-annealing treatment on the interface between the Al cathode and the active layer, again consistent with the enhanced FFs of the post-annealed devices. In this case, we could investigate through AFM the active layers of the devices prepared only under the conditions of "post-annealing-only" and "combined effect." Nevertheless, for comparison we also investigated devices prepared without post-annealing ("as-cast" and "additive-only"), but for active layers deposited on top of the poly-ethylenedioxythiophene:poly(styrenesulfonic acid) (PEDOT:PSS) layer without Al cathodes. Fig. 4a and e display the height and phase images, respectively, of the active layers of samples prepared under the "as-cast" conditions. The height image reveals a very smooth surface [root mean square (rms) variation of 0.39 nm], while the corresponding phase image suggests an inhomogeneous distribution of the donor and acceptor components in the film, without any indication of crystalline phases. The AFM images for the samples prepared under these conditions are consistent with the XRD data and with the low FF that led to the low overall PCE. Fig. 4b and f present height and phase images, respectively, of active layers containing 0.1% CP3MS without any thermal annealing ("additive-only"). Although we observe no change in roughness from the height image (rms = 0.4 nm) after adding 0.1% CP3MS, the phase image reveals a homogenous distribution of the donor and acceptor components in the film, conducive for enhanced exciton dissociation at the interface. More careful investigation of the phase image revealed fine fiber-like features of SMDPPEH and small aggregates of PCBM, representing that the early stages of the required phase separation were stimulated after the addition of 0.1% CP3MS to the blend. These results, together with the enhanced crystallinity and improved π–π stacking revealed in the XRD data and the enhanced performance (particularly the FF and value of J_{sc}) of the device prepared under these conditions, provide strong evidence for the significant role of CP3MS as a morphological controller when incorporated in the SMDPPEH:$PC_{61}BM$ blend system. Here, we consider morphological control as the "first function" exhibited by the additive CP3MS.

The working mechanism behind the role of the CP3MS as an additive enhancing the morphology might mainly be attributed to its relatively high boiling point temperature (195 °C) compared to the host solvent CB (131 °C).[28] The difference in the boiling point temperatures between CP3MS additive and CB

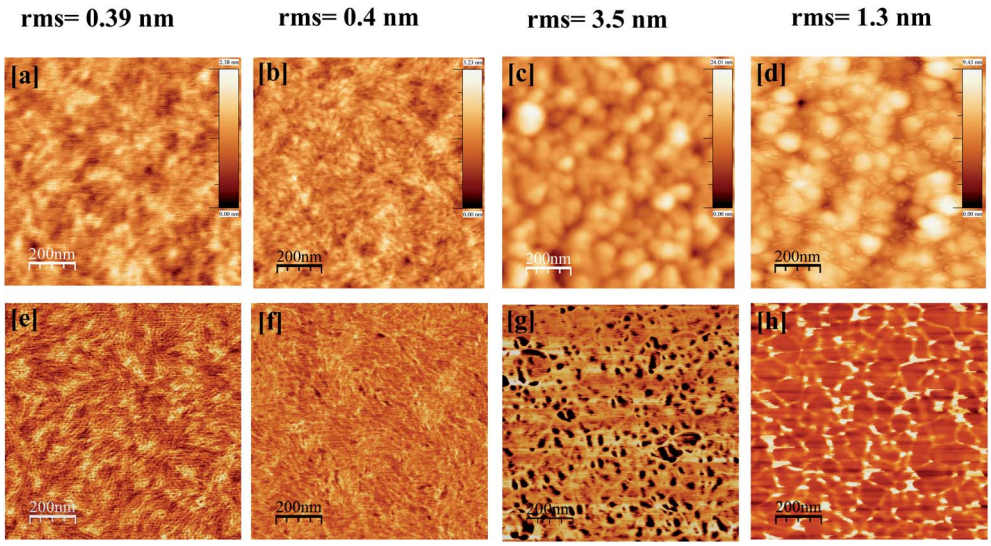

Fig. 4 AFM (a–d) height and (e–h) phase images of active layers prepared under the "as-cast," "post-annealing-only," "additive-only" and "combined effect" conditions. Image dimensions: 1 × 1 μm^2.

host solvent gives SMDPPEH donor molecules sufficient time to rearrange inside the active layer in the favorable orientation. The favorable orientation appeared clearly in the enhanced crystallinity and the appearance of fine fiber-like features after the addition of 0.1% CP3MS.

Next, we used AFM to examine the morphologies of the active layers in the post-annealed devices ("post-annealing-only" and "combined effect") after peeling off the Al cathode using sticky tape. Fig. 4c and g display height and phase images, respectively, of the morphology of the active layer obtained using the "post-annealing-only" conditions. The height image reveals a dramatic increase in roughness (rms = 3.5 nm) relative to that (rms = 0.39 nm) for the sample prepared under the "as-cast" conditions, an indication of the increased interfacial contact area between the active layer and the Al metal cap. The corresponding phase image reveals the effect of post-annealing on the morphology of the active layer. Although it contains dark spots representing strong interfacial contacts between the active layer and the Al metal cathode that were pulled-off during the Al peel-off process,[19] careful investigation revealed a developed phase separation with unevenly shaped crystalline domains of PCBM and fiber-like features of SMDPPEH. We suspected that such strong interfacial contacts at the active layer–Al cathode interface might be a reason behind the significant enhancement in the FF and the value of V_{oc} of the device prepared under these conditions. In addition, the developed phase separation, which we attribute mainly to the post-annealing effect, might also be a reason behind the enhanced overall PCE observed under these conditions. Thus, the significant enhancement in the FF and the value of V_{oc} of the device prepared under the conditions of "post-annealing-only" can be attributed to the higher quality of the defect-free interface between the active layer and the Al metal cathode. The series resistance (R_s) of this device was 1.85 Ω cm^2, relative to 2.15 Ω cm^2 for that prepared under the "as-cast" conditions. This decrease in R_s is an indication of the improved quality of the interface between the active layer and the Al cathode that resulted from post-annealing treatment.

Fig. 4d and h display height and phase images, respectively, of devices prepared under the "combined effect" conditions. In the height image, we observe a dramatic decrease in the roughness (rms = 1.3 nm) relative to that (3.5 nm) of the device prepared under the "post-annealing-only" conditions. Because we applied the same conditions for post-annealing in each case, the presence of 0.1% CP3MS was a likely factor behind the dramatic decrease in roughness. After Al peel-off, the height image in Fig. 4d reveals small islands of residuals in the valley regions of the agglomerated features. These residuals are clearly evident in the corresponding phase image, revealing the existence of bright islands only at the agglomerated domain boundaries. The phase image also reveals well-developed phase separation, with even and semi-rounded PCBM agglomerate sand fiber-like SMDPPEH, consistent with the observed high value of J_{sc} for the device prepared under these conditions. We suspect that the bright islands were the residuals of an ultrathin interlayer formed through the spontaneous migration of CP3MS in the BHJ to the interface between the active layer and the Al cathode. The dramatic decrease in the roughness of the film, relative to that of the device prepared without the additive, suggests that the formation of this ultrathin interlayer smoothed the surface and facilitated the Al peel-off process. An additional observation confirming the spontaneous formation of this ultrathin interlayer at the interface is the distinct difference between the phase images of the devices prepared with and without the additive under the same conditions of post-annealing ("post-annealing-only" and "combined effect"). Here, we follow the same analogy described by Heeger and coworkers[19] when they used the differences in phase images after Al peel-off to reveal the different responses of the active layers after post-annealing treatment. They used this approach

to confirm the positive effect of post-annealing on the interface between the active layer and Al cathode. From "post-annealing-only" and "combined effect" conditions in Fig. 4g and h, respectively: a distinct difference between the two conditions is the disappearance of the dark spots, which were an indication of the strong interactions between the active layer and the metal cathode in the case of the "post-annealing-only" sample (Fig. 4g), due to direct contact between the Al cathode and the active layers. Accordingly, the interfacial contacts between the active layer and the Al cathode were pulled-off, causing a dramatic increase in the roughness of the active layer surface in the height image and dark spots appearing in the phase image in Fig. 4c and g, respectively. In the case of the "combined effect" sample (Fig. 4h), however, the response of the active layer was totally different: the roughness decreased dramatically (from 3.5 to 1.3 nm) and the dark spots, which represented the pulled-off zones, almost disappeared, with new bright islands appearing at the agglomerated domain boundaries. These findings strongly support the notion that a smoothing agent reached the interface to dramatically decrease the roughness. We believe that this smoothing agent, which facilitated the removal of the Al cathodes during the Al peel-off process and left bright-island residuals at the domain boundaries, was an ultrathin interlayer of CP3MS molecules that migrated to the interface. This ultrathin interlayer acted as a buffer layer at the interface between the Al cathode and the active layer; we consider this phenomenon to be the "second function" performed by the CP3MS additive. Again, the value of R_s was another indication of the improvement in the quality of the interface that arose as a result of the addition of CP3MS. For example, the value of R_s decreased to 1.77 Ω cm^2 and 1.68 Ω cm^2 for the devices prepared under the "additive-only" and "combined effect" conditions, respectively, from 2.15 Ω cm^2 for the "as-cast" device. These decreases in R_s might be attributable to the migration of CP3MS to the interface between the active layer and the Al cathode, thereby decreasing the contact resistance and leading to favorable conditions for electron extraction. This behavior is consistent with the improved values of J_{sc} and FF observed for the sample prepared under these conditions relative to those of the "as-cast" sample. Fig. 5 is an additional confirmation of the spontaneous migration of CP3MS to the surface to form an ultrathin interlayer. Height images in Fig. 5a and b reveal distinct differences between the active layers prepared without and with additive, respectively; both samples were annealed at 100 °C for 10 min and both were analyzed without Al cathodes. Comparing the two images, we observe two distinct differences. The first is in the surface roughness, where the rms roughness of the active layer prepared without the additive is higher than that of the sample prepared with 0.1% CP3MS. The second is the existence of tiny wave-like features on top of the active layer containing 0.1% CP3MS; we attribute these features to the formation of an ultrathin interlayer on top of the active layer after the spontaneous migration of CP3MS to the surface. The same two differences can be clearly observed for the post-annealed devices prepared with and without the additive after Al cathode peel-off (Fig. 5c and d, respectively). These results, together with

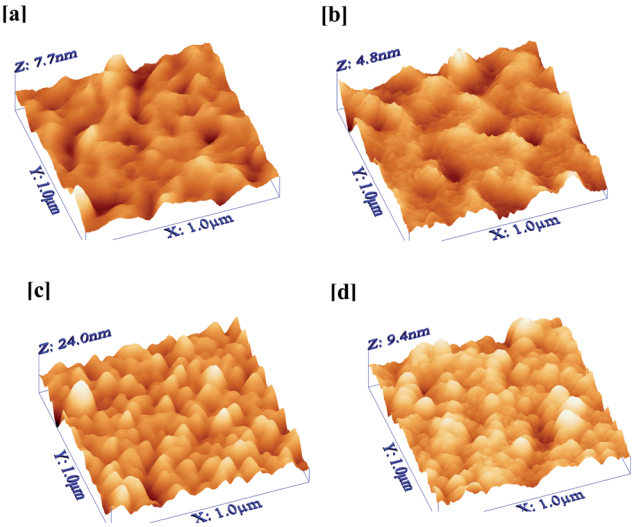

Fig. 5 (a and b) 3-D AFM height images of active layers prepared without the Al cathode: (a) without the additive and (b) with 0.1% of the CP3MS additive. (c and d) 3-D AFM height images of active layers obtained after peeling-off the Al cathode: (c) without the additive and (d) with 0.1% of the CP3MS additive. Image dimensions: 1 × 1 μm^2.

our earlier findings, confirm the formation of an ultrathin interlayer at the interface between the active layer and the Al cathode—a feature that has also been reported from previous studies.[33,41–43,45] Another noteworthy difference is the significant decrease in feature sizes for the post-annealed devices (full devices with Al cathodes) in Fig. 5c and d, relative to those in the annealed active layers prepared without Al cathodes (Fig. 5a and b). The presence of the Al metal cap effectively prevented overgrowth of the donor and acceptor materials, leading to an optimal morphology that induced a high PCE.[18]

Confirming the role of CP3MS as a buffer layer, Fig. 6a presents XPS data for the devices prepared without the additive and with 0.1% CP3MS after Al peel-off (full devices). We observe signals for Si atoms for the devices containing 0.1% CP3MS, indicative of the existence of a Si source at the interface between the Al cathode and the active layer. The only possible source for Si atoms on top of the active layer after Al peel-off was the additive CP3MS. These results confirm the migration of CP3MS to the interface between the Al cathode and the active layer under the post-annealing conditions, consistent with previously discussed AFM data and supporting our claim for the role of CP3MS as a buffer layer at the cathode interface.[33,45] Fig. 6b displays the XPS-depth profile of the active layer containing 0.1% CP3MS on top of PEDOT:PSS-coated indium tin oxide (ITO) glass. The profile reveals the existence of Si atoms at the surface and their gradual decrease at depth until vanishing. This gradual decrease in the content of Si atoms supports the existence of CP3MS at the interface and within the active layer. To further confirm the existence of Si atoms derived from the additive CP3MS at the surface, we performed XPS measurements of the active layers (*i.e.*, without Al cathodes on top) of samples containing 0.1% and 1% CP3MS after thermal annealing at 100 °C for 10 min (Fig. 6c and d respectively).

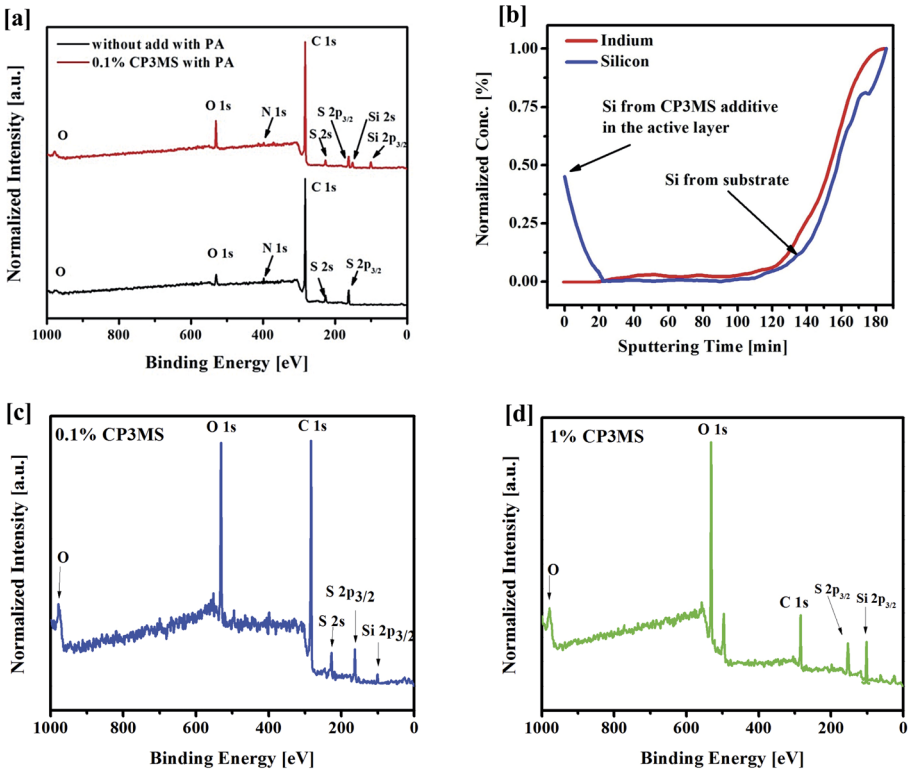

Fig. 6 XPS spectra of the active layer containing 0.1% CP3MS after peeling-off the Al cathode: (a) survey, (b) depth-profiling X-ray photoelectron spectroscopy (DP-XPS) of the active layer incorporating 0.1% CP3MS; (c) and (d) represent an XPS survey of active layers (without Al capping) containing 0.1% CP3MS and 1% CP3MS respectively.

Although (3-chloropropyl)trimethoxysilane (CP3MS; $Cl(CH_2)_3Si(OCH_3)_3$) has been used previously in organic photovoltaics as a surface modifier to change the electrode work function,[46] this paper is the first to describe its use as an additive in a BHJ organic solar cell. Our use of CP3MS as an additive is one of only a few reports of silane-based additives in BHJ solar cells.[45,47] As a silane-based molecule, CP3MS is electronically inert, it could reduce the sites of charge recombination at the interface between the Al cathode and the active layer, leading to an enhancement in the overall device performance. Because of the insulation property of CP3MS, adding an excessive amount of CP3MS results in excessively thick passivation layers that hinder electron transport from the organic layer to the metal cathode. The Si 2p signals in the XPS correspond to the Si^{3+} oxidation state shown in Fig. 6a. Partially oxidized Si species have been known for their effective hole blocking and electron tunneling capabilities.[61] Reported ultrathin SiO_2 layer was utilized as a cathode passivation layer in the field of silicon-based solar cells.[45,61] The interfacial layer containing Si–O–Si bonds generated between the active layer and Al metal cathode is expected to work as a hole-blocking passivation layer along the interface.[62] During device fabrication, vacancies and unintentional impurity formation in the active layers is unavoidable. These vacancies and impurities act as trap sites and hinder charge transport.[63] Because of the softness and inertness of CP3MS, its addition to the blend films could suppress the formation of such trap sites. This suppression prevents charges from being trapped during transport, which is consistent with previous reports.[63]

Because of its low surface energy,[33,45] CP3MS migrates to the surface, forming an ultrathin buffer layer at the interface between the active layer and the cathode. Contact angle measurements provided further supporting evidence for the migration of CP3MS to the surface. The contact angles for the active layers prepared without the additive and with 0.1% CP3MS were 97° and 108° (shown in Fig. S5a and S5b respectively; ESI†). We attribute this decrease in surface energy to the existence of CP3MS at the surface, consistent with the AFM and XPS data.

Based on our AFM, XRD, XPS, and contact angle data, Fig. 7 provides a schematic representation of the dual functions of the additive CP3MS during post-annealing treatment. Its first function was to enhance the crystallinity and morphology of the active layer through improved phase separation under the optimal conditions of post-annealing treatment and additive concentration. Its second function was the formation of an ultrathin interlayer at the interface between the active layer and Al metal cathode. These two functions of CP3MS led to simultaneous enhancements in the FF and values of V_{oc} and J_{sc}, thereby significantly increasing the overall PCE. The improved device characteristics suggest that this CP3MS buffer layer led to interfacial passivation, which suppressed charge recombination at the active layer and metal interface.

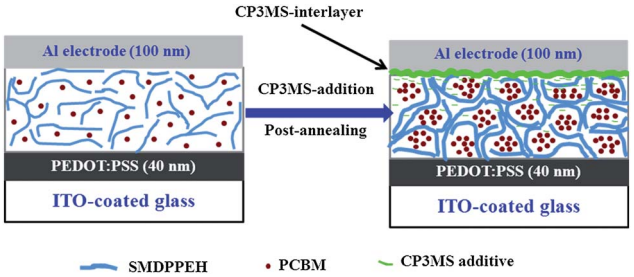

Fig. 7 Schematic representation of the dual functions of the additive CP3MS when combined with post-annealing treatment.

Interestingly, CP3MS showed its promising ability as a processing additive incorporated within other blend systems. Different CP3MS concentrations (0.05–0.2%) were added to a benzodithiophene (BDT)-based small molecule developed by our group[6] (TBDTCNR; the chemical structure is shown in Scheme S1, ESI†). Fig. S6 and Table S3 (ESI†) show that 0.1% CP3MS additive enhances the performance of TBDTCNR from 3.05% without additive to 3.8%.

3. Conclusion

A new processing additive (CP3MS) has been introduced for the first time into organic BHJ solar cells. The PCE increased significantly from 2.75% to 4.55% in the SMDPPEH:$PC_{61}BM$ blend system under the optimized conditions of CP3MS additive concentration and thermal annealing. We have observed an interesting dual function for this additive: first, as a morphological controller, confirmed from AFM and XRD data, and, second, through the formation of an ultrathin interlayer from the migration of CP3MS from the BHJ to the interface between the Al metal cathode and the active layer, confirmed from AFM, XPS, and contact angle data. We believe that this ultrathin interlayer between the active layer and the Al metal cathode acted as a buffer layer. CP3MS also showed a promising ability to enhance the performance of different blend systems. The performance of benzodithiophene (BDT)-based molecular solar cells enhanced from 3.05% without additive to 3.8% with incorporation of 0.1% CP3MS. This study introduces, for the first time, the novel concept of a dual-functional additive in the context of organic optoelectronics; the application of this type of additive is a simple and efficient approach toward enhancing the PCEs of molecular BHJ solar cells without the need for complicated syntheses of new chemical structures.

4. Experimental

4.1. Materials and solution preparation

The dialkylated diketopyrrolopyrrole chromophore (SMDPPEH, >98%) was obtained from Luminescence Technology and [6,6]-phenyl-C_{61}-butyric acid methyl ($PC_{61}BM$) ester was purchased from Solenne BV. The conducting polymer PEDOT:PSS (Clevios P VP 4083) was spin-coated to modify the ITO surface. CP3MS (Alfa Aesar) was used as a solvent additive. SMDPPEH/$PC_{61}BM$ blend solution [1 : 1 (w/w),10 mg mL^{-1} in chlorobenzene] was stirred for approximately 24 h at 70 °C in a glove box. Blend solutions of SMDPPEH:$PC_{61}BM$ were also prepared at different CP3MS concentrations (0.05–0.2%). TBDTCNR:$PC_{61}BM$ was prepared at different CP3MS concentrations (0.05–0.2%) following previous work reported elswhere.[6]

4.2. Device fabrication

Devices were fabricated on 0.1 cm^2 pre-patterned ITO-coated glass substrates (sheet resistance: 15 Ω $square^{-1}$) with the conventional device structure of ITO/PEDOT:PSS (40 nm)/SMDPPEH:$PC_{61}BM$ blend [1 : 1 (w/w),10 mg mL^{-1}]/Al(100 nm). Prior to device fabrication, the ITO-coated glass substrates were cleaned following standard procedures, including sonication in detergent followed by rinsing in deionized (DI) water. The substrates were then cleaned in UV/ozone for 15 min; the PEDOT:PSS was passed through a 0.45 μm syringe filter onto the substrates, which were then spin-coated at 4000 rpm and dried in air for 30 min at 130 °C. After the active layer had been spin-coated (1000 rpm, 1 min) inside a glove box filled with N_2, the Al cathode (100 nm) was deposited through thermal evaporation in a vacuum chamber (7×10^{-6} torr). Post-annealing of the devices was performed at different temperatures (75, 100, or 125 °C) inside a glove box filled with N_2; different annealing periods were also examined. The morphology of the active layer was studied after post-annealing. The capping Al cathode was removed gently from the top of the active layer using sticky-tape.

4.3. Device characterization

Absorption spectra of the films were measured using a Jacobs V-670 UV-Vis-NIR spectrophotometer. The photovoltaic performance of each device was measured inside a glove box filled with N_2 under simulated AM 1.5 G illumination (100 W cm^2) using a Xe lamp-based solar simulator (Thermal Oriel 1000 W). The light intensity was calibrated using a mono-silicon photodiode with a KG-5 color filter (Hamamatsu). EQE spectra were recorded under short-circuit conditions; the devices were encapsulated before they were removed for EQE measurement. The light source was a 450 W Xe lamp (Oriel Instruments, Model 6123NS). The light output from the monochromator (Oriel Instruments, Model 74100) was focused on the photovoltaic cell being tested. A Veecodi Innova atomic force microscope operated in the tapping mode was used to record the AFM images of the polymer films. XRD patterns were obtained using a PANalytical instrument. XPS was performed using a PHI 5000 Versa Probe (ULVAC-PHI, Chigasaki, Japan) equipped with an Al Ka X-ray source (1486.6 eV). Contact angles were measured using a Slideaway instrument.

Acknowledgements

We thank the ministry of education of Taiwan (through ATU program) for financial support. We also thank the National Science Council (NSC) of Taiwan (NSC 102-2221-E-001-029-MY2 and NSC 102-3113-P-009-002) and Academia Sinica Research Program for Nanoscience and Technology for financial support.

Notes and references

1 B. Kippelen and J.-L. Brédas, *Energy Environ. Sci.*, 2009, **2**, 251.
2 C. J. Brabec, N. S. Sariciftci and J. C. Hummelen, *Adv. Funct. Mater.*, 2001, **11**, 15.
3 S. Gunes, H. Neugebauer and N. S. Sariciftci, *Chem. Rev.*, 2007, **107**, 1324.
4 S. B. Darling and F. You, *RSC Adv.*, 2013, **3**, 17633.
5 B. Walker, C. Kim and T.-Q. Nguyen, *Chem. Mater.*, 2011, **23**, 470.
6 D. Patra, T. Y. Huang, C. C. Chiang, R. O. Maturana, C. W. Pao, K. C. Ho, K. H. Wei and C. W. Chu, *ACS Appl. Mater. Interfaces*, 2013, **5**, 9494.
7 D. Ye, X. Li, L. Yan, W. Zhang, Z. Hu, Y. Liang, J. Fang, W.-Y. Wong and X. Wang, *J. Mater. Chem. A*, 2013, **1**, 7622.
8 D. Patra, C.-C. Chiang, W.-A. Chen, K.-H. Wei, M.-C. Wu and C.-W. Chu, *J. Mater. Chem. A*, 2013, **1**, 7767.
9 V. Jeux, D. Demeter, P. Leriche and J. Roncali, *RSC Adv.*, 2013, **3**, 5811.
10 J. You, L. Dou, K. Yoshimura, T. Kato, K. Ohya, T. Moriarty, K. Emery, C.-C. Chen, J. Gao, G. Li and Y. Yang, *Nat. Commun.*, 2013, **4**, 1446.
11 Z. He, C. Zhong, S. Su, M. Xu, H. Wu and Y. Cao, *Nat. Photonics*, 2012, **6**, 591.
12 A. K. Kyaw, D. H. Wang, D. Wynands, J. Zhang, T. Q. Nguyen, G. C. Bazan and A. J. Heeger, *Nano Lett.*, 2013, **13**, 3796.
13 H. Hoppe and N. S. Sariciftci, *J. Mater. Chem.*, 2006, **16**, 45.
14 A. J. Moulé and K. Meerholz, *Adv. Funct. Mater.*, 2009, **19**, 3028.
15 B. P. Lyons, N. Clarke and C. Groves, *Energy Environ. Sci.*, 2012, **5**, 7657.
16 H. Waters, J. Kettle, S.-W. Chang, C.-J. Su, W.-R. Wu, U. S. Jeng, Y.-C. Tsai and M. Horie, *J. Mater. Chem. A*, 2013, **1**, 7370.
17 W. L. Leong, G. C. Welch, J. Seifter, J. H. Seo, G. C. Bazan and A. J. Heeger, *Adv. Energy Mater.*, 2013, **3**, 356.
18 P. Peumans, S. Uchida and S. R. Forrest, *Nature*, 2003, **425**, 158.
19 W. Ma, C. Yang, X. Gong, K. Lee and A. J. Heeger, *Adv. Funct. Mater.*, 2005, **15**, 1617.
20 G. Li, V. Shrotriya, Y. Yao and Y. Yang, *J. Appl. Phys.*, 2005, **98**, 043704.
21 H. Kim, W. So and S. Moon, *Sol. Energy Mater. Sol. Cells*, 2007, **91**, 581.
22 G. Li, Y. Yao, H. Yang, V. Shrotriya, G. Yang and Y. Yang, *Adv. Funct. Mater.*, 2007, **17**, 1636.
23 H. Li, Z. Chen, H. Tang, W. Xu, J. Li, X. Zhao and X. Yang, *RSC Adv.*, 2012, **2**, 10231.
24 B. Walker, A. Tamayo, D. T. Duong, X.-D. Dang, C. Kim, J. Granstrom and T.-Q. Nguyen, *Adv. Energy Mater.*, 2011, **1**, 221.
25 S. E. Shaheen, C. J. Brabec, N. S. Sariciftci, F. Padinger, T. Fromherz and J. C. Hummelen, *Appl. Phys. Lett.*, 2001, **78**, 841.
26 X. Bulliard, S.-G. Ihn, S. Yun, Y. Kim, D. Choi, J.-Y. Choi, M. Kim, M. Sim, J.-H. Park, W. Choi and K. Cho, *Adv. Funct. Mater.*, 2010, **20**, 4381.
27 P. Zhong, W. Que, Y. N. Liang, X. Yin, Y. Liao, L. B. Kong and X. Hu, *RSC Adv.*, 2013, **3**, 17904.
28 J. K. Lee, W. L. Ma, C. J. Brabec, J. Yuen, J. S. Moon, J. Y. Kim, K. Lee, G. C. Bazan and A. J. Heeger, *J. Am. Chem. Soc.*, 2008, **130**, 3619.
29 C. V. Hoven, X. D. Dang, R. C. Coffin, J. Peet, T. Q. Nguyen and G. C. Bazan, *Adv. Mater.*, 2010, **22**, E63.
30 T. Salim, L. H. Wong, B. Bräuer, R. Kukreja, Y. L. Foo, Z. Bao and Y. M. Lam, *J. Mater. Chem.*, 2011, **21**, 242.
31 J. K. Park, C. Kim, B. Walker, T.-Q. Nguyen and J. H. Seo, *RSC Adv.*, 2012, **2**, 2232.
32 K. R. Graham, R. Stalder, P. M. Wieruszewski, D. G. Patel, D. H. Salazar and J. R. Reynolds, *ACS Appl. Mater. Interfaces*, 2013, **5**, 63.
33 K. R. Graham, P. M. Wieruszewski, R. Stalder, M. J. Hartel, J. Mei, F. So and J. R. Reynolds, *Adv. Funct. Mater.*, 2012, **22**, 4801.
34 H.-Y. Chen, H. Yang, G. Yang, S. Sista, R. Zadoyan, G. Li and Y. Yang, *J. Phys. Chem. C*, 2009, **113**, 7946.
35 Y. Kim, H. R. Yeom, J. Y. Kim and C. Yang, *Energy Environ. Sci.*, 2013, **6**, 1909.
36 J. Peet, J. Y. Kim, N. E. Coates, W. L. Ma, D. Moses, A. J. Heeger and G. C. Bazan, *Nat. Mater.*, 2007, **6**, 497.
37 T. S. van der Poll, J. A. Love, T. Q. Nguyen and G. C. Bazan, *Adv. Mater.*, 2012, **24**, 3646.
38 J. A. Love, C. M. Proctor, J. Liu, C. J. Takacs, A. Sharenko, T. S. van der Poll, A. J. Heeger, G. C. Bazan and T.-Q. Nguyen, *Adv. Funct. Mater.*, 2013, **23**, 5019.
39 C. S. Kim, L. L. Tinker, B. F. DiSalle, E. D. Gomez, S. Lee, S. Bernhard and Y.-L. Loo, *Adv. Mater.*, 2009, **21**, 3110.
40 B. Lim, J. Jo, S.-I. Na, J. Kim, S.-S. Kim and D.-Y. Kim, *J. Mater. Chem.*, 2010, **20**, 10919.
41 Q. Wei, T. Nishizawa, K. Tajima and K. Hashimoto, *Adv. Mater.*, 2008, **20**, 2211.
42 F.-C. Chen and S.-C. Chien, *J. Mater. Chem.*, 2009, **19**, 6865.
43 S.-C. Chien, F.-C. Chen, M.-K. Chung and C.-S. Hsu, *J. Phys. Chem. C*, 2012, **116**, 1354.
44 J. W. Jung, J. W. Jo and W. H. Jo, *Adv. Mater.*, 2011, **23**, 1782.
45 S. Yamakawa, K. Tajima and K. Hashimoto, *Org. Electron.*, 2009, **10**, 511.
46 R. M. Cook, L.-J. Pegg, S. L. Kinnear, O. S. Hutter, R. J. H. Morris and R. A. Hatton, *Adv. Energy Mater.*, 2011, **1**, 440.
47 K. R. Graham, J. Mei, R. Stalder, J. W. Shim, H. Cheun, F. Steffy, F. So, B. Kippelen and J. R. Reynolds, *ACS Appl. Mater. Interfaces*, 2011, **3**, 1210.
48 Y. Li, P. Sonar, L. Murphy and W. Hong, *Energy Environ. Sci.*, 2013, **6**, 1684.
49 S. Qu and H. Tian, *Chem. Commun.*, 2012, **48**, 3039.
50 A. B. Tamayo, B. Walker and T.-Q. Nguyen, *J. Phys. Chem. C*, 2008, **112**, 11545.
51 A. B. Tamayo, M. Tantiwiwat, B. Walker and T.-Q. Nguyen, *J. Phys. Chem. C*, 2008, **112**, 15543.

52 B. Walker, A. B. Tamayo, X.-D. Dang, P. Zalar, J. H. Seo, A. Garcia, M. Tantiwiwat and T.-Q. Nguyen, *Adv. Funct. Mater.*, 2009, **19**, 3063.
53 J. Liu, B. Walker, A. Tamayo, Y. Zhang and T.-Q. Nguyen, *Adv. Funct. Mater.*, 2013, **23**, 47.
54 B. Walker, J. Liu, C. Kim, G. C. Welch, J. K. Park, J. Lin, P. Zalar, C. M. Proctor, J. H. Seo, G. C. Bazan and T.-Q. Nguyen, *Energy Environ. Sci.*, 2013, **6**, 952.
55 Y. Zhang, X.-D. Dang, C. Kim and T.-Q. Nguyen, *Adv. Energy Mater.*, 2011, **1**, 610.
56 J. Liu, Y. Sun, P. Moonsin, M. Kuik, C. M. Proctor, J. Lin, B. B. Hsu, V. Promarak, A. J. Heeger and T.-Q. Nguyen, *Adv. Mater.*, 2013, **25**, 5898.
57 S. Loser, C. J. Bruns, H. Miyauchi, R. P. Ortiz, A. Facchetti, S. I. Stupp and T. J. Marks, *J. Am. Chem. Soc.*, 2011, **133**, 8142.
58 O. P. Lee, A. T. Yiu, P. M. Beaujuge, C. H. Woo, T. W. Holcombe, J. E. Millstone, J. D. Douglas, M. S. Chen and J. M. Frechet, *Adv. Mater.*, 2011, **23**, 5359.
59 A. B. Tamayo, X.-D. Dang, B. Walker, J. Seo, T. Kent and T.-Q. Nguyen, *Appl. Phys. Lett.*, 2009, **94**, 103301.
60 A. Tamayo, T. Kent, M. Tantitiwat, M. A. Dante, J. Rogers and T.-Q. Nguyen, *Energy Environ. Sci.*, 2009, **2**, 1180.
61 C.-H. Lin, S. Chattopadhyay, C.-W. Hsu, M.-H. Wu, W.-C. Chen, C.-T. Wu, S.-C. Tseng, J.-S. Hwang, J.-H. Lee, C.-W. Chen, C.-H. Chen, L.-C. Chen and K.-H. Chen, *Adv. Mater.*, 2009, **21**, 759.
62 M. Han, H. Kim, H. Seo, B. Ma and J. W. Park, *Adv. Mater.*, 2012, **24**, 6311.
63 F.-C. Wu, S.-W. Hsu, H.-L. Cheng, W.-Y. Chou and F.-C. Tang, *J. Phys. Chem. C*, 2013, **117**, 8691.